Published for SISSA by Springer

Received: *April 21, 2020*
Revised: *October 27, 2020*
Accepted: *November 30, 2020*
Published: *January 20, 2021*

Measurement of the $e^+e^- \to \pi^+\pi^-$ process cross section with the SND detector at the VEPP-2000 collider in the energy region $0.525 < \sqrt{s} < 0.883$ GeV

SND collaboration

M.N. Achasov,[a,b] A.A. Baykov,[a] A.Yu. Barnyakov,[a,c] K.I. Beloborodov,[a,b] A.V. Berdyugin,[a,b] D.E. Berkaev,[a,b] A.G. Bogdanchikov,[a] A.A. Botov,[a] T.V. Dimova,[a,b] V.P. Druzhinin,[a,b] V.B. Golubev,[a] L.V. Kardapoltsev,[a,b] A.G. Kharlamov,[a,b] I.A. Koop,[a,b,c] A.A. Korol,[a,b] D.P. Kovrizhin,[a] A.S. Kupich,[a,b] A.P. Lysenko,[a] K.A. Martin,[a] N.A. Melnikova,[a] N.Yu. Muchnoi,[a,b] A.E. Obrazovsky,[a] E.V. Pakhtusova,[a] E.A. Perevedentsev,[a,b] K.V. Pugachev,[a,b] Y.S. Savchenko,[a,b] S.I. Serednyakov,[a,b] Z.K. Silagadze,[a,b] P.Yu. Shatunov,[a,b] Yu.M. Shatunov,[a,b] D.A. Shtol,[a] D.B. Shwartz,[a,b] I.K. Surin,[a] Yu.V. Usov,[a] I.M. Zemlyansky[a,b] and V.N. Zhabin[a]

[a] *Budker Institute of Nuclear Physics, Siberian Branch of the Russian Academy of Sciences, 11, Acad. Lavrentiev Pr., Novosibirsk, 630090, Russia*

[b] *Department of physics, Novosibirsk State University, 1, Pirogova str., Novosibirsk, 630090, Russia*

[c] *Novosibirsk State Technical University, 20 Prospekt K. Marksa, Novosibirsk,630073, Russia*

E-mail: a.s.kupich@inp.nsk.su

Abstract: The cross section of the process $e^+e^- \to \pi^+\pi^-$ has been measured in the Spherical Neutral Detector (SND) experiment at the VEPP-2000 e^+e^- collider VEPP-2000 in the energy region $525 < \sqrt{s} < 883$ MeV. The measurement is based on data with an integrated luminosity of about 4.6 pb^{-1}. The systematic uncertainty of the cross section determination is 0.8% at $\sqrt{s} > 0.600$ GeV. The ρ meson parameters are obtained as $m_\rho = 775.3 \pm 0.5 \pm 0.6$ MeV, $\Gamma_\rho = 145.6 \pm 0.6 \pm 0.8$ MeV, $B_{\rho\to e^+e^-} \times B_{\rho\to\pi^+\pi^-} = (4.89 \pm 0.02 \pm 0.04) \times 10^{-5}$, and the parameters of the $e^+e^- \to \omega \to \pi^+\pi^-$ process, suppressed by G-parity, as $B_{\omega\to e^+e^-} \times B_{\omega\to\pi^+\pi^-} = (1.32 \pm 0.06 \pm 0.02) \times 10^{-6}$ and $\phi_{\rho\omega} = 110.7 \pm 1.5 \pm 1.0$ degrees.

Keywords: e^+-e^- Experiments

ArXiv ePrint: 2004.00263

https://doi.org/10.1007/JHEP01(2021)113

JHEP01(2021)113

Contents

1 Introduction

SND [1, 2] is a general purpose nonmagnetic detector operating at the VEPP-2000 e^+e^- collider in the center-of-mass energy range from 0.2 to 2.0 GeV [3]. Experimental studies include measurements of the cross sections of the e^+e^- annihilation processes into hadrons. These measurements are largely motivated by the need for high-precision calculation of the hadronic contribution to the anomalous magnetic moment of the muon $(g-2)/2$ [4]. In particular, the $e^+e^- \to \pi^+\pi^-$ cross section in the energy region below 1 GeV gives the dominant contribution to this value and should be measured with accuracy better than 1% [5].

The cross section of the $e^+e^- \to \pi^+\pi^-$ process in the energy region $\sqrt{s} < 1000$ MeV can be described within the vector meson dominance model (VMD) framework and is determined by the transitions $V \to \pi^+\pi^-$ of the light vector mesons ($V = \rho, \omega, \rho', \rho''$). The main contribution in this energy region comes from the $\rho \to \pi^+\pi^-$ and from the G-parity violating $\omega \to \pi^+\pi^-$ transitions. Studies of the $e^+e^- \to \pi^+\pi^-$ reaction allow us to determine the ρ and ω meson parameters, provide information on the G-parity violation mechanism and ρ, ρ', ρ'' mixing [6].

The process $e^+e^- \to \pi^+\pi^-$ in the energy region $\sqrt{s}$ below 1000 MeV was studied for more than 40 years in a number of experiments [7–34]. This work presents the results of the $e^+e^- \to \pi^+\pi^-$ cross section measurements with SND detector in the energy region $525 < \sqrt{s} < 883$ MeV based on $IL = 4.6\,\text{pb}^{-1}$ experimental data collected by SND in 2012–2013. Approximately 2.3×10^6 collinear events are used in the analysis. About 10^6 are events of the processes $e^+e^- \to \pi^+\pi^-$, $e^+e^- \to \mu^+\mu^-$ and 1.3×10^6 are $e^+e^- \to e^+e^-$ events.

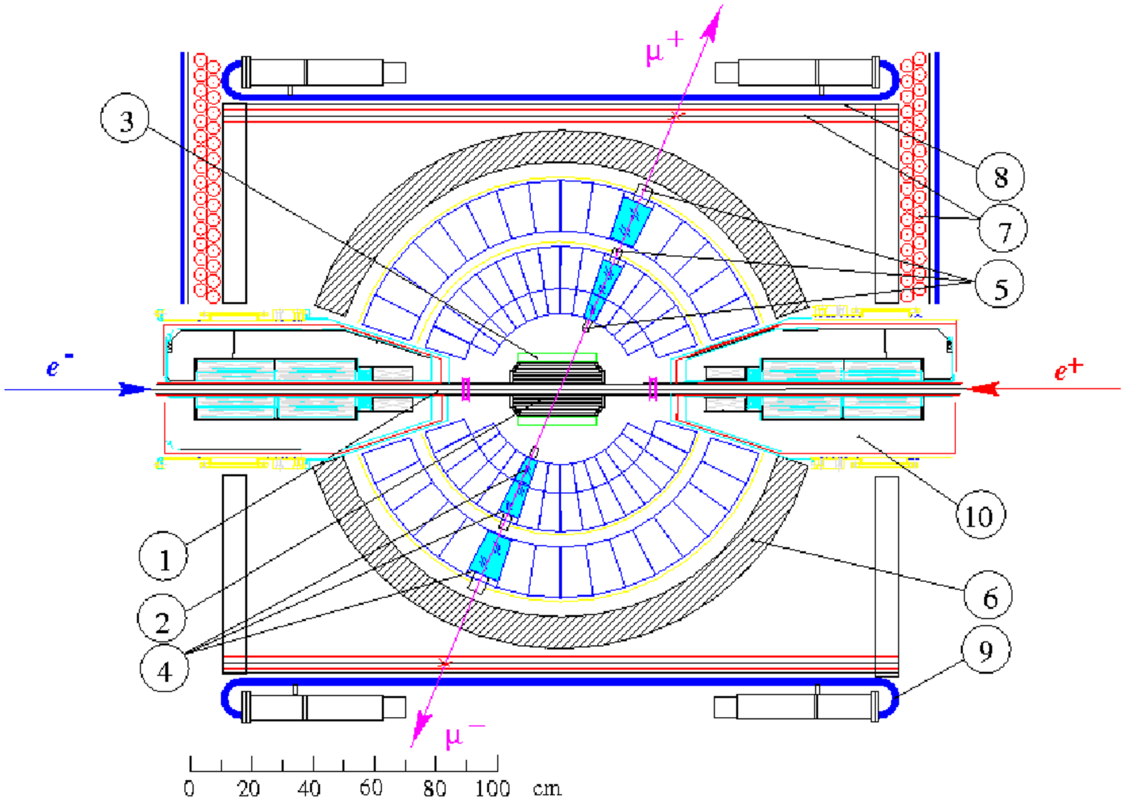

Figure 1. SND detector, section along the beams: (1) beam pipe, (2) tracking system, (3) aerogel Cherenkov counters, (4) NaI (Tl) crystals, (5) vacuum phototriodes, (6) iron absorber, (7) proportional tubes, (8) iron absorber, (9) scintillation counters, (10) solenoids of collider.

2 Experiment

The SND is operated at the VEPP-2000 collider since 2010 till present day. It consists of a tracking system based on cylindrical drift and proportional chambers placed in a common gas volume, aerogel threshold counters [35], a three-layer spherical electromagnetic calorimeter based on NaI (Tl) crystals and a muon system which includes two layers of proportional tubes and scintillation counters (figure 1). The calorimeter energy and angular resolutions depend on the photon energy E as $\sigma_E/E(\%) = 4.2\%/\sqrt[4]{E(\mathrm{GeV})}$ and $\sigma_{\phi,\theta} = 0.82^\circ/\sqrt{E(\mathrm{GeV})} \oplus 0.63^\circ$. Its total solid angle is 95% of 4π. The solid angle of the tracking system is 94% of 4π. Its angular resolution is 0.45° and 0.8° for the azimuthal and polar angles, respectively. The threshold Cherenkov counters are based on aerogel with the refractive index of 1.05. The threshold momenta for $e/\mu/\pi$ are approximately equal to 1.6/330/436 MeV/c, respectively. This system covers 60% of the total solid angle.

The VEPP-2000 collider beam energy is determined using a beam-energy-measurement system based on the Compton back-scattering of laser photons on the electron beam. The accuracy of the beam-energy measurement is about 30 keV [36, 37].

3 Analysis

The cross section of the process $e^+e^- \to \pi^+\pi^-$ is measured as follows.

1. The collinear $e^+e^- \to e^+e^-, \pi^+\pi^-, \mu^+\mu^-$ events are selected.

2. The selected events are sorted into the two classes: e^+e^- and $\pi^+\pi^-, \mu^+\mu^-$ using the energy depositions in the calorimeter crystals.

3. The luminosity is determined from the number of $e^+e^- \to e^+e^-$ events:

$$IL = \frac{N_{ee}}{\varepsilon_{ee}\sigma_{ee}}. \tag{3.1}$$

   Here N_{ee}, ε_{ee} and σ_{ee} are the number of events, detection efficiency and cross section of the process $e^+e^- \to e^+e^-$ respectively. To obtain the number of $e^+e^- \to \pi^+\pi^-$ events, the number of $e^+e^- \to \mu^+\mu^-$ events is calculated using theoretical cross section as

$$N_{\mu\mu} = IL\varepsilon_{\mu\mu}\sigma_{\mu\mu} \tag{3.2}$$

   and then subtracted from the total number of $\pi^+\pi^-$ and $\mu^+\mu^-$ events. Here $\varepsilon_{\mu\mu}$ and $\sigma_{\mu\mu}$ are the detection efficiency and cross section of $e^+e^- \to \mu^+\mu^-$, respectively.

4. The Born cross section of the process $e^+e^- \to \pi^+\pi^-$ is calculated using formula:

$$\sigma^0_{\pi\pi} = \frac{N_{\pi\pi}}{IL\varepsilon_{\pi\pi}(1+\delta_r)}. \tag{3.3}$$

   Here $1+\delta_r$ is a radiative correction, $N_{\pi\pi}$ and $\varepsilon_{\pi\pi}$ are the number of events and the detection efficiency for the process $e^+e^- \to \pi^+\pi^-$.

The detection efficiency for each process is derived from the Monte Carlo simulation based on GEANT4 [38, 39]. Apparatus effects such as electronics noise, signal pile-up, actual time and amplitude resolutions of electronics channels, the bad channels are taken into account in the simulation.

Generation of $e^+e^- \to e^+e^-$, $\mu^+\mu^-$ and $\pi^+\pi^-$ events is performed by the MCGPJ [40] generator. It is based on formulae from [41, 42]. The generator takes into account initial and final state radiation (ISR and FSR), as well as Coulomb interaction in the final state. It allows one to calculate cross sections and radiative corrections with accuracy $\sigma_{\rm rad} = 0.2\%$. The simulation of the process $e^+e^- \to e^+e^-$ is performed with the cut on the polar angles of the final electron and positron $30^\circ < \theta_{e^\pm} < 150^\circ$.

The $e^+e^- \to e^+e^-$, $\mu^+\mu^-$ and $\pi^+\pi^-$ events have different distributions of the energy deposition over calorimeter crystals. In $e^+e^- \to e^+e^-$ events the electrons and positrons produce electromagnetic showers, with the most probable energy losses of about 0.92 of the initial particle energy. Muons lose their energy by ionization of the calorimeter material through which they pass. The charged pions lose energy due to ionization and nuclear interaction with the detector material. The separation parameter of $e^+e^- \to e^+e^-$ and

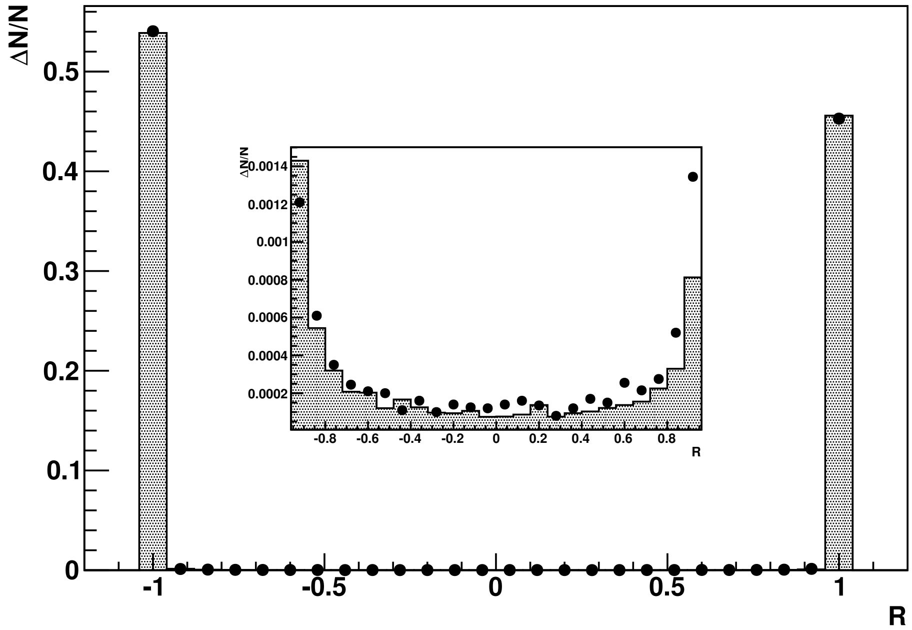

Figure 2. The distribution of the separation parameter R for all collinear events ($e^+e^- \to e^+e^-$, $\pi^+\pi^-$ and $\mu^+\mu^-$) at the energy $\sqrt{s}$ =778 MeV. The insert depicts the same histograms in the region between the peaks. Dots – experiment, histogram – simulation. Histogram for MC simulation is sum of distributions for $e^+e^- \to \mu^+\mu^-$, e^+e^- and $\pi^+\pi^-$ events. The contribution of each process to the histogram was calculated according to cross sections used in MCGPJ generator [40].

$e^+e^- \to \pi^+\pi^-$ events (R) in the energy region $\sqrt{s} = 0.5$–1.0 GeV is based on the differences in the energy deposition profiles. It was developed using machine learning method [43]. The distribution of the separation parameter R is shown in figure 2. The $e^+e^- \to e^+e^-$ events are located in the region $R < 0$, while $e^+e^- \to \pi^+\pi^-, \mu^+\mu^-$ events are located at $R > 0$.

3.1 Events selection

During the data taking, the first-level trigger selects events with one or more tracks in the drift chamber and with the total energy deposition in the calorimeter greater than 100 MeV. During processing of the experimental data, event reconstruction is performed [1]. For the further analysis the collinear events are selected using the following criteria.

1. The number of charged particles $N_{\text{cha}} \geq 2$. An event can also contain additional neutral particles due to beam background, nuclear interaction of charged pions, splitting of electromagnetic showers and initial and final state radiation.

2. $|\Delta\theta| = |180^\circ - (\theta_1 + \theta_2)| < 12^\circ$ and $|\Delta\phi| = |180^\circ - |\phi_1 - \phi_2|| < 4^\circ$, where $\theta_{1,2}$ and $\phi_{1,2}$ are the polar and azimuthal angles of charged particles with the largest energy deposition (particles in the event are ordered by the energy deposition), respectively.

3. $E_{1,2} > 40\,\text{MeV}$, where E_i is the energy deposition of the ith charged particle.

4. $50^\circ < \theta_0 < 130^\circ$, where $\theta_0 = (\theta_1 - \theta_2 + 180^\circ)/2$.

5. $|r_{1,2}| < 1\,\text{cm}$, where r_i is the distance between the track of the ith particle and the beam axis.

6. $|z_{1,2}| < 8\,\text{cm}$, where z_i is the coordinate of the ith particle vertex (point of the track closest to the beam axis) along the beams axis.

7. The muon system veto is used for suppressing the cosmic background.

3.2 Subtraction of $e^+e^- \to \pi^+\pi^-\pi^0$ and cosmic background

In the event sample selected under these conditions, one has $e^+e^- \to e^+e^-$, $\pi^+\pi^-$, $\mu^+\mu^-$ events, residual cosmic background, and a small contribution from $e^+e^- \to \pi^+\pi^-\pi^0$ reaction at $\sqrt{s} \approx m_\omega$.

The number of background events from the process $e^+e^- \to \pi^+\pi^-\pi^0$ is estimated as

$$N_{3\pi} = n_{3\pi} \times \frac{M_{3\pi}}{m_{3\pi}}, \tag{3.4}$$

where $M_{3\pi}$ is a number of simulated $e^+e^- \to \pi^+\pi^-\pi^0$ events selected using the nominal conditions for collinear events, described above, $n_{3\pi}$ and $m_{3\pi}$ are the number of data and simulated events, respectively, selected under conditions:

1. $N_{\text{cha}} \geq 2$.

2. The number of neutral particles $N_{\text{neu}} \geq 2$.

3. $|\Delta\theta| > 10^\circ$ and $|\Delta\phi| > 10^\circ$.

4. $40^\circ < \theta_{1,2} < 140^\circ$.

5. $\chi^2_{3\pi} < 30$, where $\chi^2_{3\pi}$ is the χ^2 of the kinematic fit of the event under $e^+e^- \to \pi^+\pi^-\pi^0$ hypothesis.

It is found that the $e^+e^- \to \pi^+\pi^-\pi^0$ background is maximal in the energy point $\sqrt{s} = 782.9\,\text{MeV}$, where its fraction is less than 0.15%, corresponding to 37 background events.

The cosmic events are suppressed by the muon system. The z coordinate distribution of the production point for collinear events is shown in figure 3. The e^+e^- annihilation events have a Gaussian distribution peaked at $z = 0$, while the cosmic distribution is nearly uniform. As figure 3 shows, the muon subsystem veto (veto = 1) separates cosmic muons from the e^+e^- annihilation events.

The number of the residual cosmic events is estimated as follows

$$N_{\text{cosm}} = N_{\text{data}}^{\text{veto=1}} \frac{N_{\text{cosm}}^{\text{veto=0}}}{N_{\text{cosm}}^{\text{veto=1}}}, \tag{3.5}$$

where $N_{\text{data}}^{\text{veto=1}}$ is the number of collinear events selected using the nominal selection criteria, but with veto = 1, $N_{\text{cosm}}^{\text{veto=0}}$ and $N_{\text{cosm}}^{\text{veto=1}}$ are the numbers of cosmic events with veto = 1 and veto = 0, respectively. Two types of cosmic events are used:

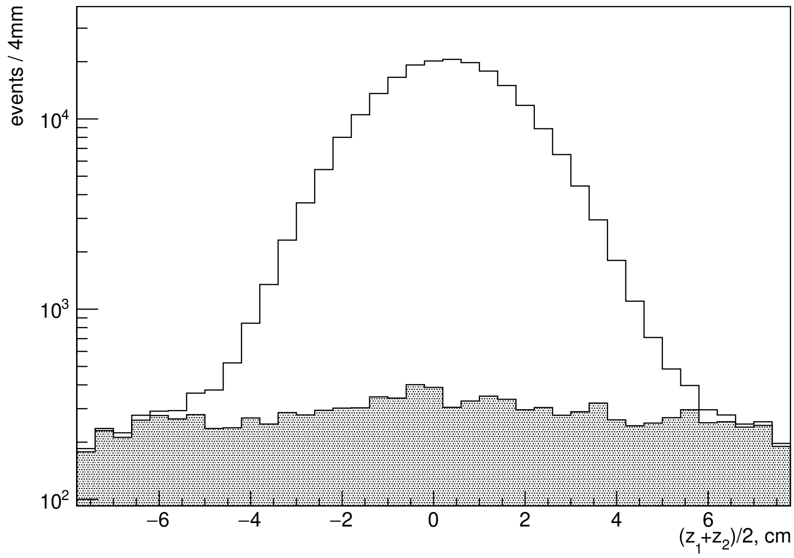

Figure 3. The distributions of the z coordinate of the charged particle vertex for collinear events at $\sqrt{s} = 778\,\mathrm{MeV}$. The histogram represents events without muon system veto (veto = 0), while the shaded histogram shows events with muon system veto.

1. Collinear events with additional cuts: $|r_{1,2}| > 0.5$ cm and $|z_{1,2}| > 5\,\mathrm{cm}$.

2. Events recorded in special cosmic runs satisfying the nominal selection criteria.

In both cases, the ratio $N_{\mathrm{cosm}}^{\mathrm{veto}=0}/N_{\mathrm{cosm}}^{\mathrm{veto}=1}$ is found to be equal to $2.5\% \pm 0.1\%$.

3.3 Detection efficiency

The $\Delta\phi$ and $\Delta\theta$ distributions for the $e^+e^- \to e^+e^-$ and $e^+e^- \to \pi^+\pi^-$ events are shown in figures 4, 5, 6 and 7. There are small differences in the shapes of the data and simulated spectra. The following values are used as a measure of the systematic uncertainty due to the $\Delta\theta$ and $\Delta\phi$ cuts:

$$\delta_x = \frac{R_x^{\pi\pi}}{R_x^{ee}}, \quad x = \Delta\phi(\Delta\theta). \tag{3.6}$$

Here

$$R_{\Delta\phi}^i = \frac{N_i(|\Delta\phi| < 4^\circ)}{N_i(|\Delta\phi| < 8^\circ)} \Big/ \frac{M_i(|\Delta\phi| < 4^\circ)}{M_i(|\Delta\phi| < 8^\circ)}, \tag{3.7}$$

$$R_{\Delta\theta}^i = \frac{N_i(|\Delta\theta| < 12^\circ)}{N_i(|\Delta\theta| < 18^\circ)} \Big/ \frac{M_i(|\Delta\theta| < 12^\circ)}{M_i(|\Delta\theta| < 18^\circ)}, \tag{3.8}$$

where $i = \pi\pi(ee)$, N_i and M_i are the numbers of data and simulated events selected under the conditions on $\Delta\phi$ and $\Delta\theta$ indicated in parentheses. The $\delta_{\Delta\theta}$ and $\delta_{\Delta\phi}$ do not depend on energy. Their deviations from unity are taken as systematic errors. Thus the systematic uncertainty associated with the $\Delta\phi$ and $\Delta\theta$ cuts is $\sigma_\Delta = 0.001 \oplus 0.002 \approx 0.002$.

JHEP01(2021)113

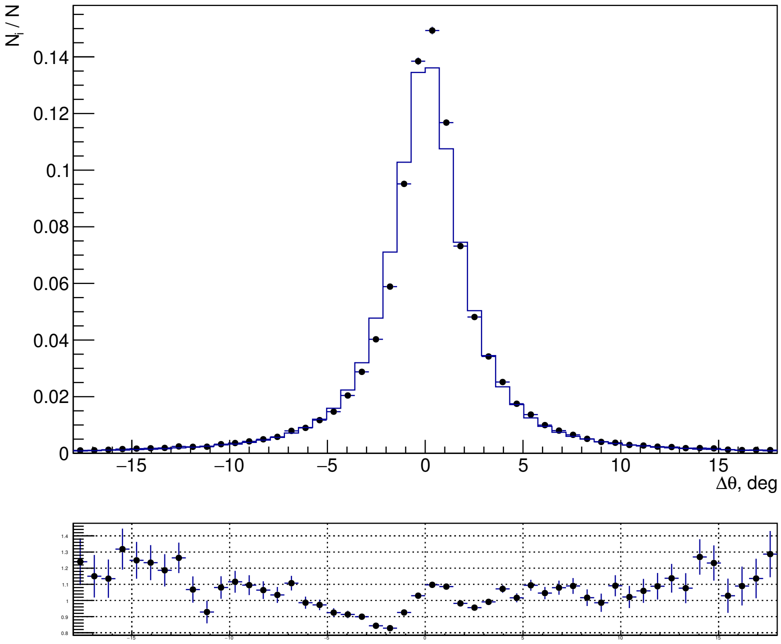

Figure 4. The $\Delta\theta$ distribution for $e^+e^- \to \pi^+\pi^-$ events at $\sqrt{s} = 778\,\text{MeV}$. The solid histogram represents simulation, while the dotted histogram shows data. Their ratio depicted below.

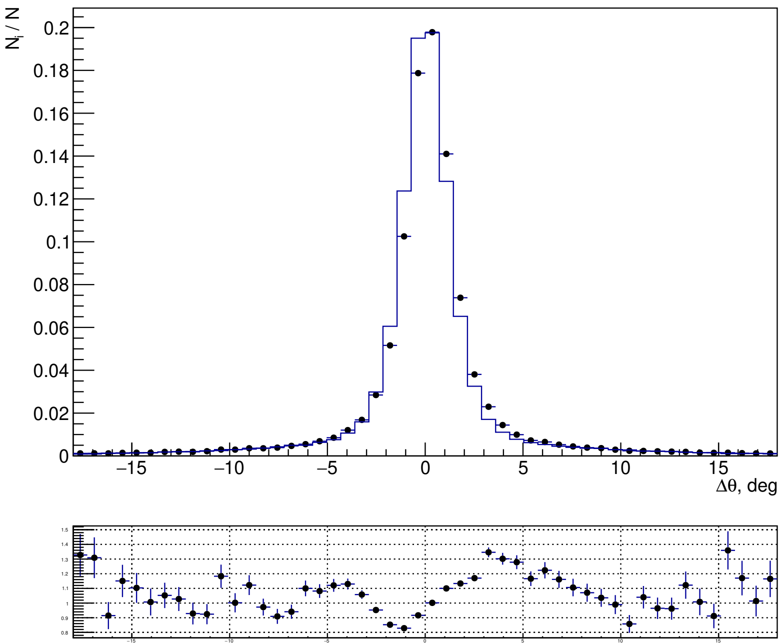

Figure 5. The $\Delta\theta$ distribution for $e^+e^- \to e^+e^-$ events at $\sqrt{s} = 778\,\text{MeV}$. The solid histogram represents simulation, while the dotted histogram shows data. Their ratio depicted below.

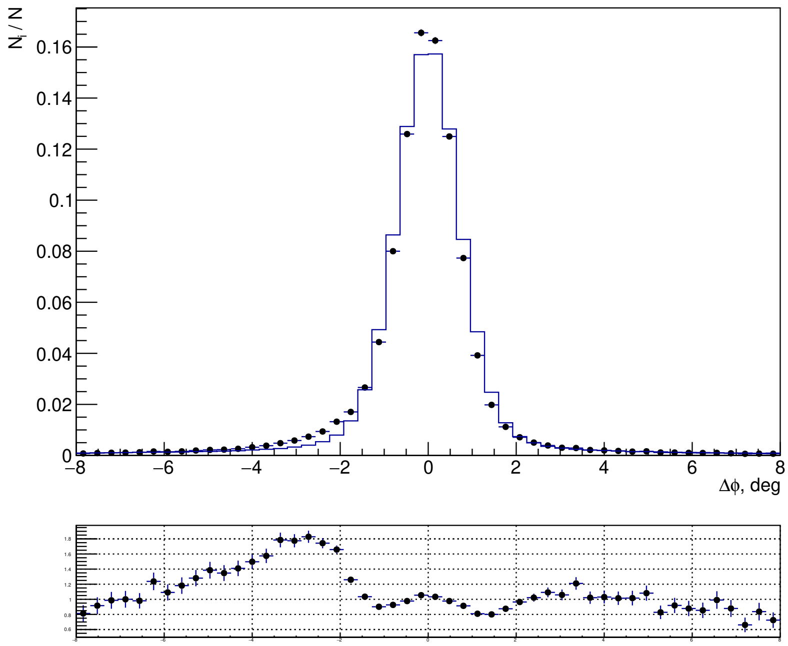

Figure 6. The $\Delta\phi$ distribution for $e^+e^- \to \pi^+\pi^-$ events at $\sqrt{s} = 778\,\mathrm{MeV}$. The solid histogram represents simulation, while the dotted histogram shows data. Their ratio depicted below.

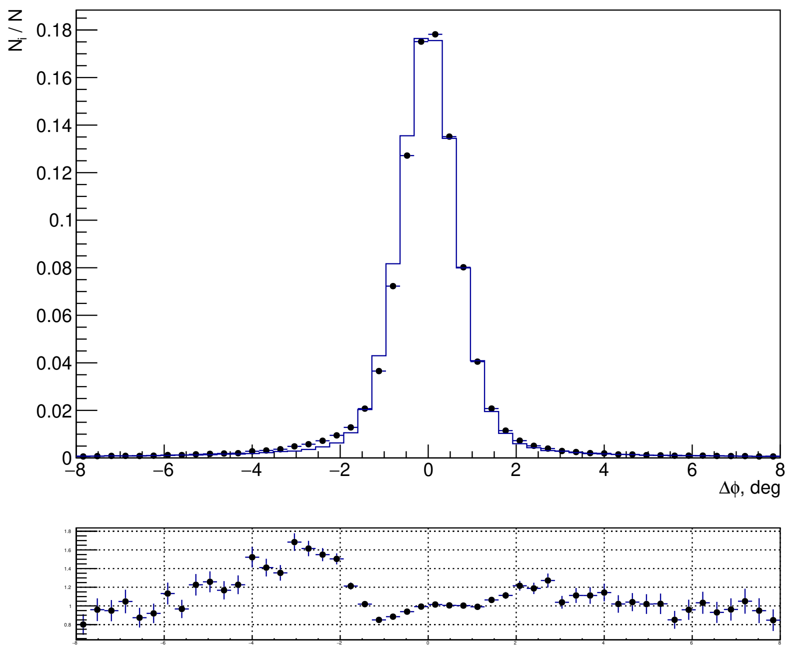

Figure 7. The $\Delta\phi$ distribution for $e^+e^- \to e^+e^-$ events at $\sqrt{s} = 778\,\mathrm{MeV}$. The solid histogram represents simulation, while the dotted histogram shows data. Their ratio depicted below.

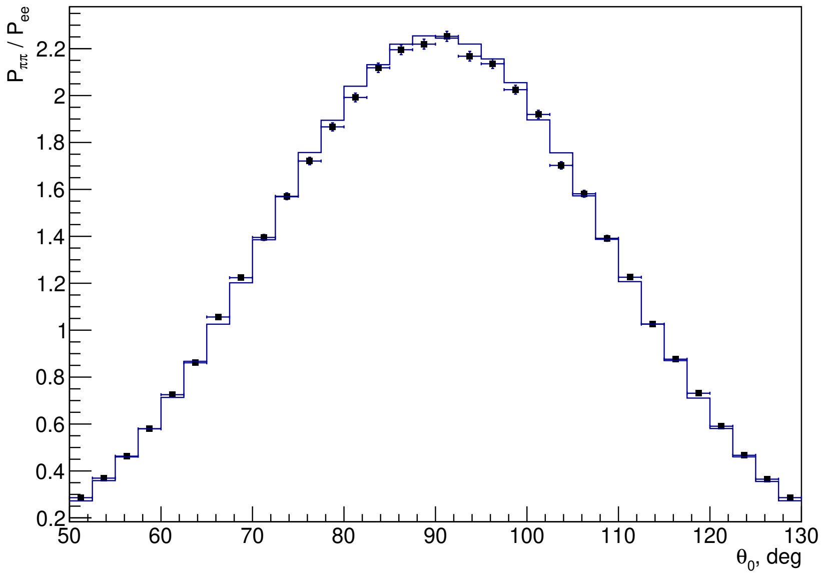

Figure 8. The ratio of θ_0 distributions of $e^+e^- \to \pi^+\pi^-$ and $e^+e^- \to e^+e^-$ events. Histogram – simulation, dots – experiment.

The ratio of the θ_0 distributions for the $e^+e^- \to \pi^+\pi^-$ and $e^+e^- \to e^+e^-$ events is shown in figure 8. There are some differences between these ratios for data and simulated distributions. To estimate the systematic error due to the θ_0 cut, the following ratio is used:

$$\delta_\theta = \frac{\delta(\theta_x)}{\delta(50^\circ)}, \quad 40^\circ < \theta_x < 55^\circ, \tag{3.9}$$

where

$$\delta(\theta_x) = \frac{N_{\pi\pi}(\theta_x < \theta < 180^\circ - \theta_x)}{N_{ee}(\theta_x < \theta < 180^\circ - \theta_x)} \Big/ \frac{M_{\pi\pi}(\theta_x < \theta < 180^\circ - \theta_x)}{M_{ee}(\theta_x < \theta < 180^\circ - \theta_x)}. \tag{3.10}$$

Here $N_{\pi\pi}(\theta_x < \theta_0 < 180^\circ - \theta_x)$, $N_{ee}(\theta_x < \theta_0 < 180^\circ - \theta_x)$, $M_{\pi\pi}(\theta_x < \theta_0 < 180^\circ - \theta_x)$, $M_{ee}(\theta_x < \theta_0 < 180^\circ - \theta_x)$ are the numbers of $e^+e^- \to \pi^+\pi^-$ and $e^+e^- \to e^+e^-$ events summed over all energy points in experiment and simulation with $\theta_x < \theta_0 < 180^\circ - \theta_x$. The largest deviation of δ_{θ_0} from unity is equal to 0.005 (figure 9). This value is taken as a systematic error σ_θ associated with $50^\circ < \theta_0 < 130^\circ$ cut.

Imperfection in simulation of pion nuclear interactions implies that the cut on the particle energy deposition leads to an inaccuracy in the detection efficiency of the $e^+e^- \to \pi^+\pi^-$ process. To take this inaccuracy into account, the detection efficiency is multiplied by the correction coefficient. The correction coefficient is obtained by using pseudo $\pi\pi$ events, which are constructed using events of the processes $e^+e^- \to \omega(\phi) \to \pi^+\pi^-\pi^0$ and $e^+e^- \to \pi^+\pi^-$ [43]. The corrections obtained using different types of pseudo events differ less than 0.005, they do not depend on the pion energy and their average is equal to 0.992. As a result, the correction coefficient is set equal to 0.992, and the difference is taken as a systematic error $\sigma_E = 0.005$.

JHEP01(2021)113

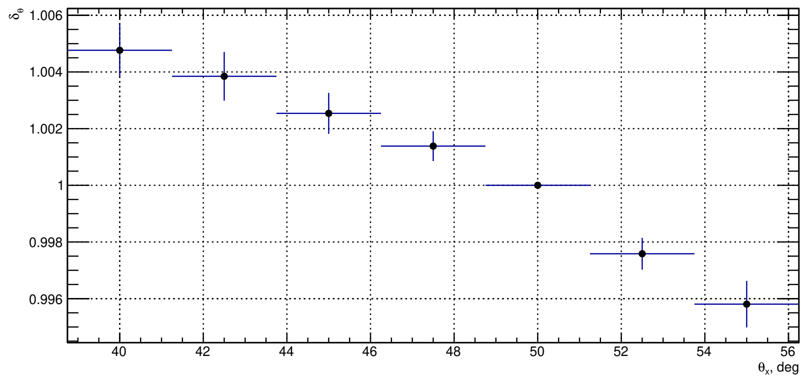

Figure 9. The δ_θ dependence on θ_x (3.10).

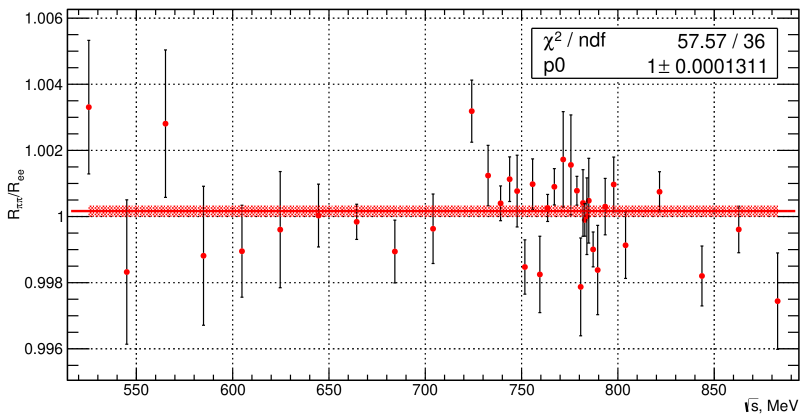

Figure 10. The $R_{\pi\pi}/R_{ee}$ dependence on $\sqrt{s}$. Line depicts an average value.

In the tracking system, the particle track can be lost due to reconstruction inefficiency. The probabilities $\varepsilon_{\pi\pi}^{\text{data}}$ and $\varepsilon_{ee}^{\text{data}}$ to find two tracks in the $e^+e^- \to \pi^+\pi^-$ and $e^+e^- \to e^+e^-$ events are determined using experimental data. Their ratio to probabilities derived from simulated events

$$R_i = \frac{\varepsilon_j^{\text{data}}}{\varepsilon_j^{mc}}, \quad i = ee, \pi\pi \tag{3.11}$$

can vary significantly in the different energy points. But the ratio $R_{\pi\pi}/R_{ee}$, which contributes to the measured cross section, is energy independent and equal to unity with error 10^{-4} (figure 10).

Pions can be lost due to the nuclear interaction in the detector material before the tracking system. The probability of pion loss is studied using $e^+e^- \to \pi^+\pi^-\pi^0$ events. It was found that the difference between these values in data and simulation is 0.002, which is taken as a systematic error $\sigma_{\text{nucl}} = 0.2\%$.

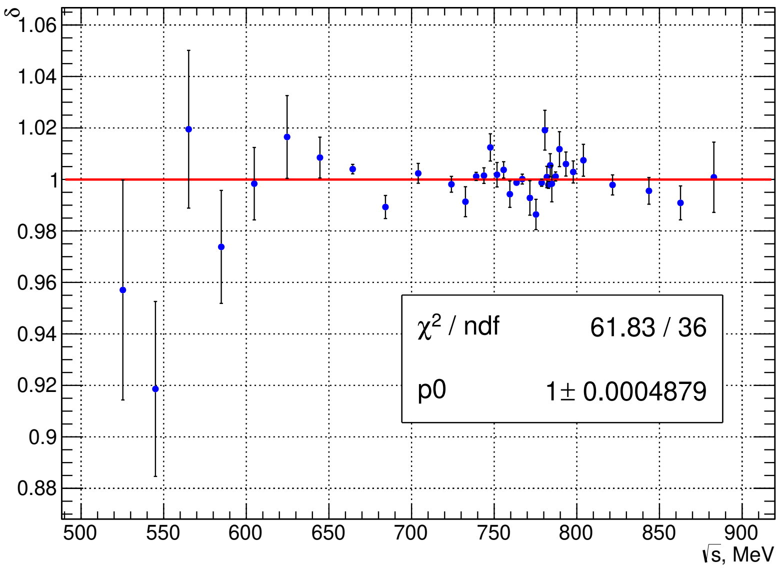

Figure 11. The δ_{veto} dependence on $\sqrt{s}$. Line depicts an average value.

The use of the muon system veto for event selection (veto = 0) leads to inaccuracy in the determination of the measured cross section due to the uncertainty in the simulation of the muons and pions traversing the detector. To obtain the necessary corrections, the events close to the median plane $0^\circ < \phi < 14^\circ$, $166^\circ < \phi < 194^\circ$, $360^\circ > \phi > 346^\circ$), where the cosmic background is minimal, are used. The correction is the ratio of the $e^+e^- \to \pi^+\pi^-$ cross sections measured with (veto = 0) and without (veto ≥ 0) using the muon system:

$$\delta_{\text{veto}} = \frac{\sigma_{\pi\pi}(\text{veto} \geq 0)}{\sigma_{\pi\pi}(\text{veto} = 0)}. \tag{3.12}$$

In the case of veto ≥ 0, a contribution of the residual cosmic muons background is estimated from the fit to the $(z_1 + z_2)/2$ spectrum with a sum of the Gaussian and uniform distributions. The δ_{veto} does not dependent on energy and its average value is consistent with 1 (figure 11). This indicates the absence of the systematic error related to the condition veto = 0. Relatively high $\chi^2/n.d.f$ in figures 11 (1.71) and 10 (1.6) is due to the large devitions of 2–3 energy points. It's caused by background contamination of the control samples (events with veto ≥ 0 or only one reconstructed track) used in δ_{veto} and $R_{\pi\pi}/R_{ee}$ calculations.

Trigger efficiency is greater than 99.9% for all types of collinear events due to the energy deposition cuts $E_{1,2} > 40\,\text{MeV}$. These cuts provide performance of the energy deposition threshold. Therefore systematic uncertainty from trigger inefficiency is considered to be negligible.

Uncertainties in simulation of energy depositions in the calorimeter can lead to an inaccuracy in e/π discrimination. The identification efficiency and related systematic error were studied in [43] using pseudo-$\pi\pi$ and pseudo-ee events. It varies with energy from

JHEP01(2021)113

0.996 to 0.998 for the $e^+e^- \to e^+e^-$ events and from 0.994 to 0.998 for the $e^+e^- \to \pi^+\pi^-$ events. The systematic error $\sigma_{\rm PID}$ of the $e^+e^- \to \pi^+\pi^-$ cross section measurement due to cuts R< 0.0 and R> 0.0 does not exceed 0.002 at $\sqrt{s} > 650$ MeV. Below 650 MeV, the $\sigma_{\rm PID}$ value increases with decrease of energy and reaches 0.005 at $\sqrt{s} = 525.1$ MeV.

3.4 Calculation of the cross section

The number of selected events in the regions R >0 and R <0 are:

$$N_a = IL(\sigma_{\pi\pi}\varepsilon^a_{\pi\pi} + \sigma_{\mu\mu}\varepsilon^a_{\mu\mu} + \sigma_{ee}\varepsilon^a_{ee}) + N^a_{nc}, \tag{3.13}$$

where index $a = 1, 2$ indicates the events with 0< R and R >0 respectively; σ_{jj} and ε^a_{jj} are physical cross section and detection efficiency of the process with jj = $\pi^+\pi^-, \mu^+\mu^-, e^+e^-$ in the final state, N^a_{nc} is a number of $e^+e^- \to \pi^+\pi^-\pi^0$ and cosmic background events, IL is the integrated luminosity. The detection efficiencies ε^a_{jj} take into account the correction coefficients described above. Using the formula for N_a, the $e^+e^- \to \pi^+\pi^-$ cross section is calculated as

$$\sigma_{\pi\pi}(s_i) = \frac{N_1 - N^1_{nc} - IL\sigma_{\mu\mu}\varepsilon^1_{\mu\mu}(s_i) - \sigma_{ee}\varepsilon^1_{ee}}{IL\varepsilon^1_{\pi\pi}}, \tag{3.14}$$

where

$$IL = \frac{(N_2 - N^2_{nc})\varepsilon^1_{\pi\pi} - (N_1 - N^1_{nc})\varepsilon^2_{\pi\pi}}{\sigma_{ee}(\varepsilon^2_{ee}\varepsilon^1_{\pi\pi} - \varepsilon^1_{ee}\varepsilon^2_{\pi\pi}) + \sigma_{\mu\mu}(\varepsilon^2_{\mu\mu}\varepsilon^1_{\pi\pi} - \varepsilon^1_{\mu\mu}\varepsilon^2_{\pi\pi})}. \tag{3.15}$$

Subtraction of the $e^+e^- \to \mu^+\mu^-$ background leads to additional contribution to the systematic error, which is estimated as follows:

$$\sigma_\mu = (\sigma_\theta \oplus \sigma_\Delta \oplus \sigma_{\rm rad}) \times \frac{\varepsilon^1_{\mu\mu}\sigma_{\mu\mu}}{\varepsilon^1_{\pi\pi}\sigma_{\pi\pi}}. \tag{3.16}$$

The Born cross section for the $e^+e^- \to \pi^+\pi^-$ process is calculated from as

$$\sigma^0_{\pi\pi}(s_i) = \frac{\sigma_{\pi\pi}(s_i)}{1 + \delta_{\rm rad}(s_i)}. \tag{3.17}$$

The radiative correction $\delta_{\rm rad}(s_i)$, which takes into account the initial and final states radiation, is calculated using the MCGPJ generator. The value of $\delta_{\rm rad}(s)$ depends on the $\sigma^0_{\pi\pi}(s)$ cross section at lower energies, and it is therefore calculated iteratively. The iteration stops when its value changes by less than 0.05% in consecutive iterations. The correction for the center of mass energy spread is taken into account also. The spread does not exceed 0.3 MeV in the energy region below 1 GeV, and the correction is less than 0.1%.

The measured cross section $\sigma^0_{\pi\pi}$ is presented in table 1. The systematic errors of the cross section determination are listed in table 2.

3.5 Fit to the measured cross section

In the framework of the vector meson dominance model, the cross section of the $e^+e^- \to \pi^+\pi^-$ process is

$$\sigma^0_{\pi\pi}(s) = \frac{2}{3}\frac{\alpha^2}{s^{5/2}}P_{\pi\pi}(s)|A_{\pi\pi}(s)|^2, \tag{3.18}$$

$\sqrt{s}$, MeV	$\sigma_{\pi\pi}$, nb	$\sigma^0_{\pi\pi}$, nb	$\lvert F(s)\rvert^2$	$\sigma_{\rm bare}$, nb
525.1	203.4±12.3±2.4	210.4±12.7±2.5	4.4±0.3±0.1	209.7±12.7±2.5
544	224.4±10.1±2.5	232.5±10.5±2.6	5±0.2±0.1	231.9±10.4±2.6
565.2	235±12.3±2.4	244.3±12.8±2.5	5.5±0.3±0.1	243.8±12.8±2.5
585	254.2±10.7±2.5	265±11.1±2.6	6.2±0.3±0.1	264.8±11.1±2.6
604.8	328.8±8.7±3	344.7±9.2±3.1	8.3±0.2±0.1	344.8±9.2±3.1
624.8	366.4±11.1±3.2	386.1±11.7±3.4	9.7±0.3±0.1	386.7±11.7±3.4
644.6	438±8.2±3.7	464.2±8.7±3.9	12.1±0.2±0.1	465.6±8.7±3.9
664.5	525.9±3.5±4.4	561.3±3.7±4.7	15.3±0.1±0.1	563.7±3.7±4.7
684.4	642.1±8.4±5.3	689.1±9±5.6	19.5±0.3±0.2	692.9±9.1±5.7
704.2	798.1±10.3±6.5	860.7±11.1±7	25.4±0.3±0.2	865.5±11.1±7
724.1	1030.4±9.5±8.3	1112.6±10.3±9	34.2±0.3±0.3	1116.6±10.3±9
739.1	1146.4±5.6±9.2	1233.7±6±9.9	39.1±0.2±0.3	1234±6±9.9
743.8	1200.9±9.8±9.7	1289.4±10.6±10.4	41.3±0.3±0.3	1288.1±10.6±10.4
747.7	1215±14.4±9.8	1301.6±15.4±10.5	42±0.5±0.3	1298.7±15.4±10.5
751.7	1199.4±13.7±9.7	1281.4±14.7±10.3	41.7±0.5±0.3	1276.6±14.6±10.3
755.7	1246.5±10.8±10	1327.9±11.5±10.7	43.5±0.4±0.4	1321.3±11.4±10.6
759.6	1288.3±17.3±10.4	1368±18.3±11	45.2±0.6±0.4	1360.3±18.2±10.9
763.6	1263.4±5±10.2	1336.8±5.2±10.8	44.5±0.2±0.4	1328.9±5.2±10.7
767.8	1249.1±6.9±10.1	1317±7.2±10.6	44.2±0.2±0.4	1310±7.2±10.5
771.6	1290.3±22.2±10.4	1356.5±23.3±10.9	45.9±0.8±0.4	1351.7±23.2±10.9
775.7	1290.9±17.2±10.4	1353.6±18±10.9	46.2±0.6±0.4	1353.2±18±10.9
778.6	1257±5.3±10.1	1311.1±5.5±10.5	45±0.2±0.4	1307.4±5.5±10.5
780.7	1198.9±18.4±9.7	1229.2±18.9±9.9	42.3±0.7±0.3	1211.4±18.6±9.8
782	1104.8±11.2±8.9	1106.9±11.2±8.9	38.2±0.4±0.3	1074.7±10.9±8.7
782.9	1058.1±4.8±8.5	1039.8±4.7±8.4	36±0.2±0.3	999±4.5±8
783.7	1004.9±11.6±8.1	971.9±11.3±7.8	33.7±0.4±0.3	925.2±10.7±7.5
784.7	959.2±12.8±7.7	916.8±12.2±7.4	31.9±0.4±0.3	865.8±11.6±7
786.7	913.5±5.1±7.4	872.3±4.8±7	30.4±0.2±0.2	819.1±4.5±6.6
789.5	934.6±14.1±7.5	903.1±13.7±7.3	31.7±0.5±0.3	850.9±12.9±6.9
793.9	890.4±10±7.2	867.8±9.7±7	30.7±0.3±0.2	823.1±9.2±6.6
797.7	858.9±10.1±6.9	836.3±9.9±6.7	29.8±0.4±0.2	795.8±9.4±6.4
804	819.5±10.5±6.6	791.4±10.1±6.4	28.6±0.4±0.2	755.4±9.6±6.1
821.8	654.8±5.6±5.3	608.7±5.2±4.9	22.8±0.2±0.2	583±5±4.7
843.4	496.6±5.8±4	438±5.1±3.6	17.1±0.2±0.1	420.4±4.9±3.4
862.7	382.2±4.6±3.1	321.2±3.9±2.6	13±0.2±0.1	309±3.7±2.5
883.2	303.2±6.7±2.5	242.1±5.3±2	10.2±0.2±0.1	233.5±5.1±1.9

Table 1. The results of the $e^+e^- \to \pi^+\pi^-$ cross section measurements. $\sigma_{\pi\pi}$, $\sigma^0_{\pi\pi}$ and $F(s)$ are the physical, Born cross sections of the process $e^+e^- \to \pi^+\pi^-$, and pion form factor, calculated with formula in ref. [25]. $\sigma_{\rm bare}$ is the $e^+e^- \to \pi^+\pi^-$ undressed cross section without vacuum polarization, but with the final state radiative correction. Both statistical and systematic errors are shown.

JHEP01(2021)113

Error	at $\sqrt{s} > 600\,\text{MeV}$, %	at $\sqrt{s} \leq 600\,\text{MeV}$, %
σ_{PID}	0.1–0.2	0.3–0.5
σ_{μ}	0.0–0.2	0.3–0.7
σ_{Δ}	0.2	
σ_{θ}	0.5	
σ_{E}	0.5	
σ_{rad}	0.2	
σ_{nucl}	0.2	
total	0.8	0.9–1.2

Table 2. Various contributions to the systematic error of the $e^+e^- \to \pi^+\pi^-$ cross section measurement.

where $P_{\pi\pi}(s)$ is the phase space factor:

$$P_{\pi\pi}(s) = q_\pi^3(s), \quad q_\pi(s) = \frac{1}{2}\sqrt{s - 4m_\pi^2}. \tag{3.19}$$

The transition amplitudes are given by

$$|A_{\pi\pi}(s)|^2 = \left| \sqrt{\frac{3}{2}} \frac{1}{\alpha} \sum_{V=\rho,\omega,\rho'} \frac{\Gamma_V m_V^3 \ \sqrt{m_V \sigma(V \to \pi^+\pi^-)}}{D_V(s)} \frac{e^{i\phi_{\rho V}}}{\sqrt{q_\pi^3(m_V)}} \right|^2, \tag{3.20}$$

where

$$D_V(s) = m_V^2 - s - i\ \sqrt{s}\Gamma_V(s), \tag{3.21}$$

$$\Gamma_V(s) = \sum_f \Gamma(V \to f, s). \tag{3.22}$$

Here, f denotes the final state of the vector meson V decay, m_V is the vector meson mass, $\Gamma_V = \Gamma_V(m_V)$ and $\phi_{\rho V}$ is the relative interference phase between the vector mesons V and ρ, and, hence, $\phi_{\rho\rho} = 0$.

The following forms of the energy dependence of the vector meson total widths are used:

$$\Gamma_\omega(s) = \frac{m_\omega^2}{s} \frac{q_\pi^3(s)}{q_\pi^3(m_\omega)} \Gamma_\omega B_{\omega\to\pi^+\pi^-} + \frac{q_{\pi\gamma}^3(s)}{q_{\pi\gamma}^3(m_\omega)} \Gamma_\omega B_{\omega\to\pi^0\gamma} + \frac{W_{\rho\pi}(s)}{W_{\rho\pi}(m_\omega)} \Gamma_\omega B_{\omega\to 3\pi}, \tag{3.23}$$

$$\Gamma_V(s) = \frac{m_V^2}{s} \frac{q_\pi^3(s)}{q_\pi^3(m_V)} \Gamma_V \quad (V = \rho, \rho'). \tag{3.24}$$

Here, $q_{\pi\gamma} = (s - m_\pi^2)/2\sqrt{s}$, $W_{\rho\pi}(s)$ is the phase space factor for the $\rho\pi \to \pi^+\pi^-\pi^0$ final state [45], $B_{V\to f}$ is the branching fraction of the vector meson decay to the final state f. In the energy dependence of the ρ and ρ' mesons widths only the $V \to \pi^+\pi^-$ decays are taken into account. Such approach is justified in the energy region $\sqrt{s} < 1000\,\text{MeV}$. The

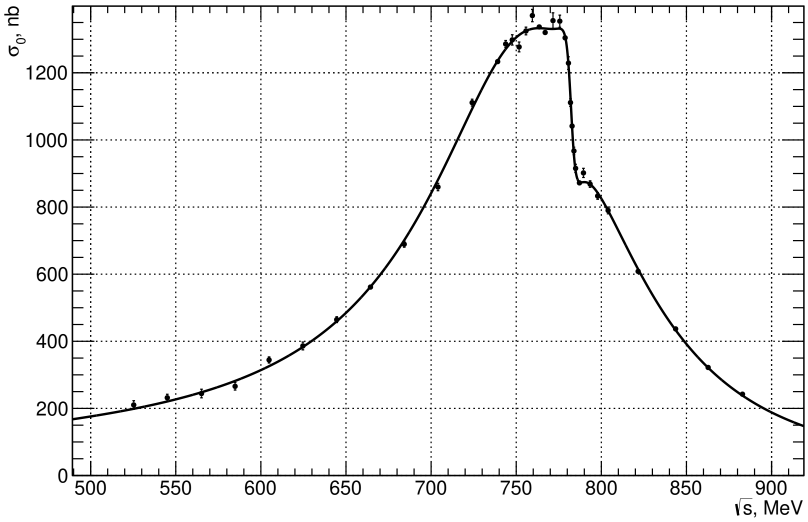

Figure 12. The dependence of the Born cross section of the $e^+e^- \to \pi^+\pi^-$ process on energy, dots with errors are data, curve is the fit result.

relative decay probabilities are calculated as follows

$$B_{V\to f} = \frac{\sigma(V \to f)}{\sigma(V)}, \tag{3.25}$$

$$\sigma(V) = \sum_f \sigma(V \to f), \tag{3.26}$$

$$\sigma(V \to f) = \frac{12\pi B_{V\to e^+e^-} B_{V\to f}}{m_V^2}. \tag{3.27}$$

The fit to the measured cross section $\sigma^0_{\pi\pi}$ is performed with the following free parameters m_ρ, Γ_ρ, $\sigma(\rho \to \pi^+\pi^-)$, $\sigma(\omega \to \pi^+\pi^-)$, $\sigma_(\rho' \to \pi^+\pi^-)$ and $\phi_{\rho\omega}$. The values of m_ω, Γ_ω, $m_{\rho'}$, $\Gamma_{\rho'}$ are taken from [46]. The relative phase $\phi_{\rho\rho'}$ is fixed at π according to ref. [25]. Only uncorrelated errors of the cross section are taken into account in the fit. The results of the fit (figure 12) together with the results of the SND measurements at the VEPP-2M collider [26] are presented in table 3. The products

$$B_{V\to e^+e^-} \times B_{V\to\pi^+\pi^-} = \frac{m_V^2 \sigma(V \to \pi^+\pi^-)}{12\pi} \quad (V = \rho, \omega) \tag{3.28}$$

are also presented in table 3.

The ratio between the measured cross section and the fit curve is shown in figure 13. The systematic errors of m_ρ and Γ_ρ are related to the model uncertainty. It is estimated by comparison of the central values of these parameters presented in table 3 with the results of the fit with a model based on the Gounaris-Sakurai parametrization [27, 42]. If the m_ω and Γ_ω are free parameters of the fit, their values are in agreement with those presented in PDG [46], and the value of $\phi_{\rho\omega}$ is shifted by 1°. This difference is taken as the systematic uncertainty of the $\phi_{\rho\omega}$.

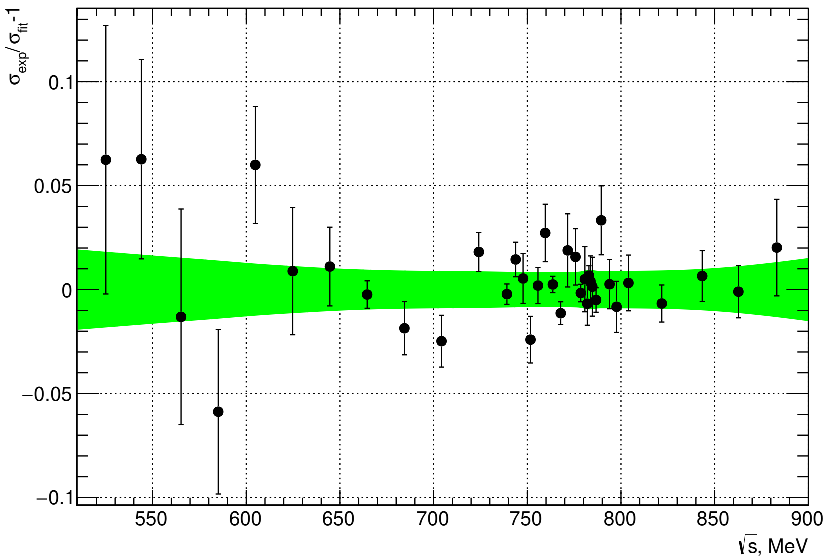

Figure 13. The relative difference between the measured $e^+e^- \to \pi^+\pi^-$ cross section and the fit curve.

Parameter	This work	SND06
m_ρ, MeV	$775.3 \pm 0.5 \pm 0.6$	$774.6 \pm 0.4 \pm 0.5$
Γ_ρ, MeV	$145.6 \pm 0.6 \pm 0.8$	$146.1 \pm 0.8 \pm 1.5$
$\sigma(\rho \to \pi^+\pi^-)$, nb	$1189.7 \pm 4.5 \pm 9.5$	$1193 \pm 7 \pm 16$
$\sigma(\omega \to \pi^+\pi^-)$, nb	$31.5 \pm 1.2 \pm 0.6$	$29.3 \pm 1.4 \pm 1.0$
$\phi_{\rho\omega}$, deg.	$110.7 \pm 1.1 \pm 1.0$	$113.7 \pm 1.3 \pm 2.0$
$\sigma(\rho' \to \pi^+\pi^-)$, nb	2.4 ± 0.6	1.8 ± 0.2
χ^2/ndf	$47/30$	–
$B_{\rho\to e^+e^-} \times B_{\rho\to\pi^+\pi^-}$	$(4.889 \pm 0.015 \pm 0.039)\ \times 10^{-5}$	$(4.876 \pm 0.023 \pm 0.064)\ \times 10^{-5}$
$B_{\omega\to e^+e^-} \times B_{\omega\to\pi^+\pi^-}$	$(1.318 \pm 0.051 \pm 0.021)\ \times 10^{-6}$	$(1.225 \pm 0.058 \pm 0.041)\ \times 10^{-6}$

Table 3. Results of the fit obtained in this work together with results from ref. [26] (SND06). Both statistical and systematic errors are shown.

3.6 Contribution to the a_μ

The contribution to the anomalous magnetic moment of the muon due to $\pi^+\pi^-(\gamma)$ intermediate state in the vacuum polarization is calculated via the dispersion integral

$$a_\mu(\pi\pi, 525\,\text{MeV} \leq \sqrt{s} \leq 883\,\text{MeV}) = \left(\frac{\alpha m_\mu}{3\pi}\right)^2 \int_{S_{\min}}^{S_{\max}} \frac{R(s)K(s)}{s^2} ds, \tag{3.29}$$

where $K(s)$ is the known kernel [47] and

$$R(s) = \frac{\sigma_{\text{bare}}}{\sigma(e^+e^- \to \mu^+\mu^-)}, \tag{3.30}$$

$$\sigma(e^+e^- \to \mu^+\mu^-) = \frac{4\pi\alpha^2}{3s}. \tag{3.31}$$

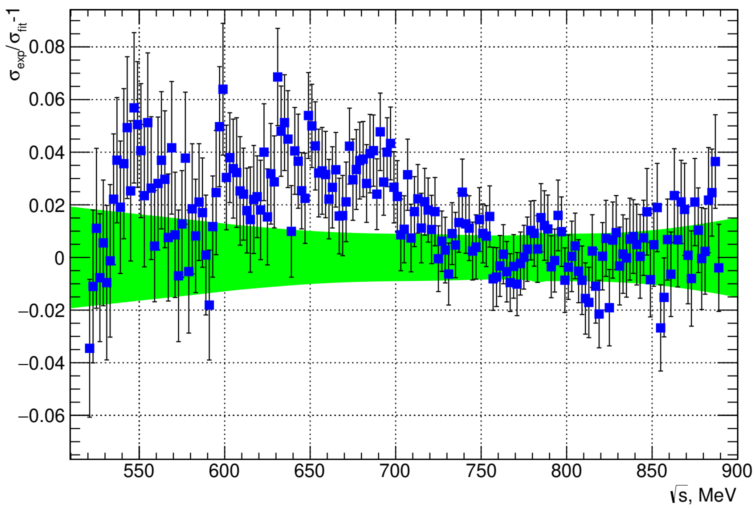

Figure 14. The relative difference between the $e^+e^- \to \pi^+\pi^-$ cross section measured by BaBar [32] and the fit to the SND data. The error bars take into account both statistic and systematical errors of BaBar data. The shaded area corresponds to the quadratic sum of the systematic and statistical errors of the SND.

Here σ_{bare} (table 1) is the bare cross section of the process $e^+e^- \to \pi^+\pi^-$ (the cross section without vacuum polarization contribution but taking into account the final state correction):

$$\sigma_{\text{bare}}(s) = \sigma^0_{\pi\pi}(s) \times |1 - \Pi(s)|^2 \times \left(1 + \frac{\alpha}{\pi}a(s)\right), \tag{3.32}$$

where $\Pi(s)$ is the polarization operator calculated according to the ref. [41] from the known $e^+e^- \to$ hadrons cross section [48]. The last factor $a(s)$ takes into account the final state radiation for the point-like pion [49].

The integral (3.29) is evaluated by using the trapezoidal rule. As a result it is obtained

$$a_\mu(\pi\pi, 525\,\text{MeV} \le \sqrt{s} \le 883\,\text{MeV}) = (409.79 \pm 1.44 \pm 3.87) \times 10^{-10}.$$

The difference 1.8×10^{-10} between this value and one, calculated with a fit curve, is taken as additional source of the systematics.

4 Discussion

The comparison of the $e^+e^- \to \pi^+\pi^-$ cross section obtained in this work with the results [25, 28, 32, 50] is shown in figure 14, 15, 16. The difference of 3% between SND and BABAR data is observed in the energy region $0.62 \ge \sqrt{s} \le 0.7$ GeV, while outside it the SND and BABAR data are consistent (figure 14). The deviation between the KLOE and SND data is 1–3% at $\sqrt{s} \ge$0.7 GeV. Below 0.7 GeV, the measurements are consistent (figure 15). The results obtained in this work and in experiments at VEPP-2M are in agreement (figure 16).

The parameters of the ρ and ω mesons obtained in this analysis are consistent with the results of [26] (table 3). The ρ meson mass m_ρ is in agreement with the results of earlier

JHEP01(2021)113

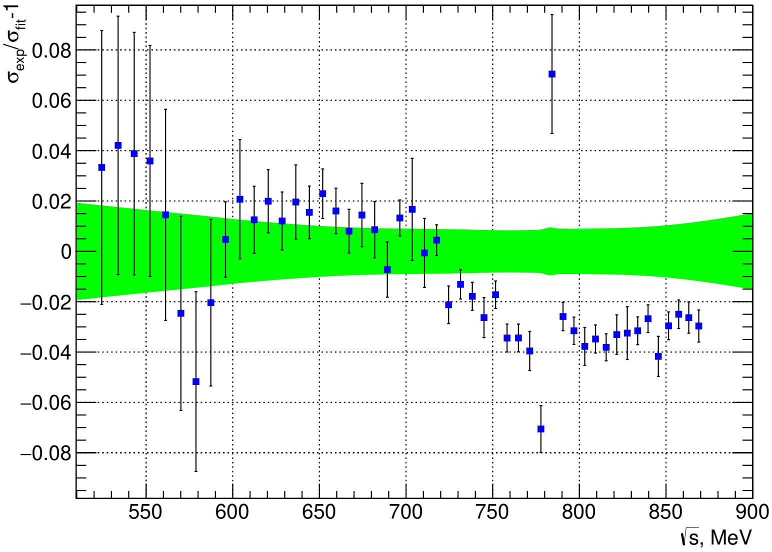

Figure 15. The relative difference between the $e^+e^- \to \pi^+\pi^-$ cross section measured by KLOE [50] and the fit to the SND data. The error bars take into account both statistic and systematical errors of KLOE data. The shaded area corresponds to the quadratic sum of the systematic and statistical errors of the SND.

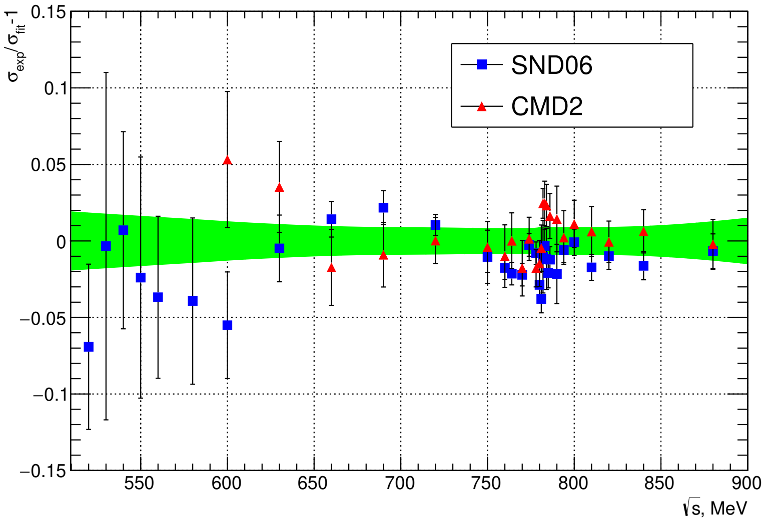

Figure 16. The relative difference between the $e^+e^- \to \pi^+\pi^-$ cross sections measured by SND [26] and CMD-2 [28] at VEPP-2M and the fit to the SND data at VEPP-2000. The error bars take into account both statistic and systematical errors of VEPP-2M data. The shaded area corresponds to the quadratic sum of the systematic and statistical errors of the SND at VEPP-2000.

experiments [26, 28, 32, 51] (figure 17). Its width Γ_ρ agrees with results of refs. [26, 28, 51] and contradict to the value reported by BaBar [32] (figure 18). To understand the source of the latter difference, we perform BABAR cross section fit in the energy region 0.525–0.883 GeV using our model (3.18). The obtained ρ meson width is 147.38 MeV $\pm$ 0.47 MeV.

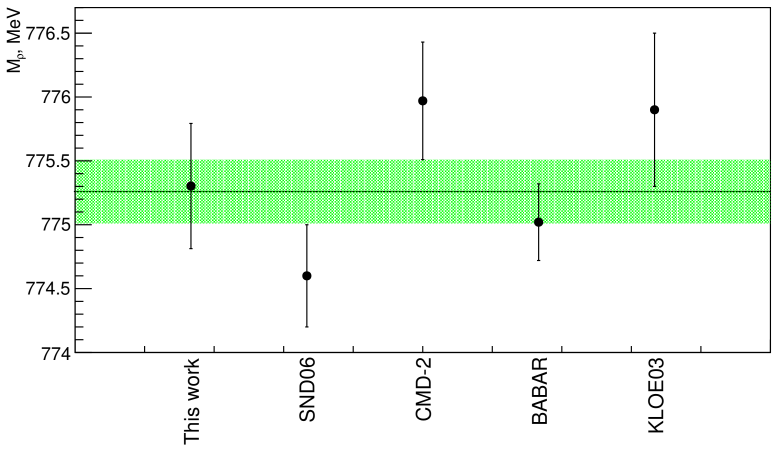

Figure 17. The ρ meson mass m_ρ measured in this work and in refs. [26, 28, 32, 51]. The shaded area shows the PDG value [46].

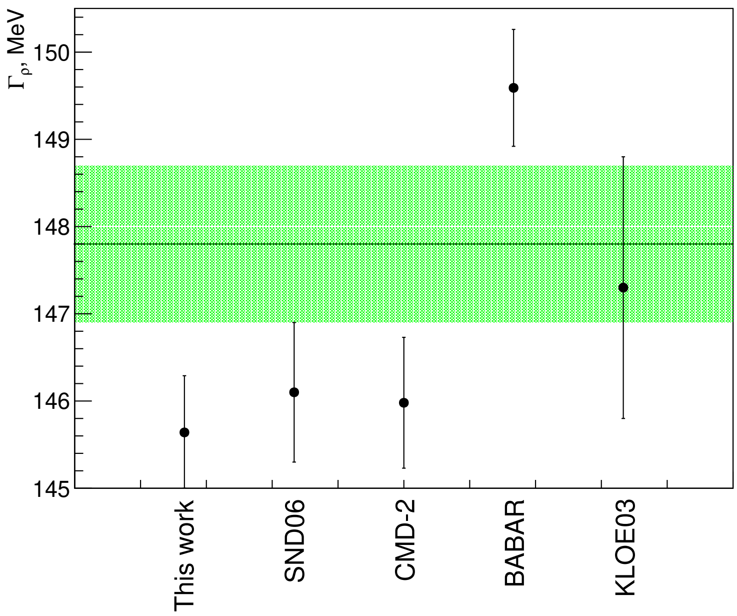

Figure 18. The ρ meson width Γ_ρ measured in this work and in refs. [26, 28, 32, 51]. The shaded area shows the PDG value [46].

We conclude that the discrepancy can be partially explained by difference between the fitting models.

The differences between $a_\mu(\pi\pi, 525\text{MeV} \leq \sqrt{s} \leq 883\text{MeV}) \times 10^{10}$ obtained in this work and those derived from [26, 32] do not exceed one standard deviation, and there is a discrepancy between KLOE [29–31] and SND results (table 4).

Measurement	$a_\mu(\pi\pi) \times 10^{10}$
This work	$409.79 \pm 1.44 \pm 3.87$
SND06	$406.47 \pm 1.74 \pm 5.28$
BaBar	$413.58 \pm 2.04 \pm 2.29$
KLOE	$403.39 \pm 0.72 \pm 2.50$

Table 4. The contribution to the anomalous magnetic moment of the muon $a_\mu(\pi\pi, 525\text{MeV} \leq \sqrt{s} \leq 883\text{MeV}) \times 10^{10}$ derived from the SND and [26, 32, 50] data. The covariance matrix is used to calculate the statistical uncertainty for [32, 50].

5 Conclusion

The cross section of the process $e^+e^- \to \pi^+\pi^-$ has been measured in the SND experiment at the VEPP-2000 collider in the energy region $525 < \sqrt{s} < 883$ MeV. The systematic error of the measurement is 0.8% at $\sqrt{s} > 600$ MeV and 0.9–1.2 % at $\sqrt{s} < 600$ MeV. The measured cross section has been analyzed in the framework of the generalized vector meson dominance model. The following ρ meson parameters have been obtained:

$$m_\rho = 775.3 \pm 0.5 \pm 0.6\,\text{MeV},$$
$$\Gamma_\rho = 145.6 \pm 0.6 \pm 0.8\,\text{MeV},$$
$$B_{\rho\to e^+e^-} \times B_{\rho\to\pi^+\pi^-} = (4.89 \pm 0.02 \pm 0.04) \times 10^{-5}.$$

The parameters of the G-parity suppressed process $e^+e^- \to \omega \to \pi^+\pi^-$ has been measured:

$$B_{\omega\to e^+e^-} \times B_{\omega\to\pi^+\pi^-} = (1.32 \pm 0.06 \pm 0.02) \times 10^{-6},$$

the relative phase between ρ and ω mesons

$$\phi_{\rho\omega} = (110.7 \pm 1.5 \pm 1.0)^\circ.$$

The result of this work is in agreement with VEPP-2M measurements, but is in conflict with BaBar and KLOE measurements. The $\pi^+\pi^-(\gamma)$ contribution to the anomalous magnetic moment of the muon has been derived from the measured cross section: $a_\mu(\pi\pi, 525\,\text{MeV} \leq \sqrt{s} \leq 883\,\text{MeV}) = (409.79 \pm 1.44 \pm 3.87) \times 10^{-10}$.

Acknowledgments

The authors are grateful to B. Malaescu and A. Keshavarzi for useful discussions. The work is supported in part by grants RFBR 18-02-00382-a, 18-02-00147-a, 20-02-00347-a, 20-02-00139-a, 20-02-00060-a.

References

[1] M.N. Achasov et al., *Spherical neutral detector for VEPP-2M collider*, *Nucl. Instrum. Meth. A* **449** (2000) 125 [hep-ex/9909015] [INSPIRE].

[2] M.N. Achasov et al., *Spherical Neutral Detector for experiments at VEPP-2000 e^+e^- collider*, in proceedings of *International Workshop on ee collisions from Phi to Psi*, Novosibirsk Russia (2011) [*Nucl. Phys. B Proc. Suppl.* **225-227** (2012) 66] [INSPIRE].

[3] D.E. Berkaev et al., *Electron-positron collider VEPP-2000. First experiments*, *Zh. Eksp. Teor. Fiz.* **140** (2011) 247.

[4] I. Logashenko et al., *The Measurement of the Anomalous Magnetic Moment of the Muon at Fermilab*, *J. Phys. Chem. Ref. Data* **44** (2015) 031211.

[5] I.B. Logashenko et al., *Measurement of the hadronic cross sections at Novosibirsk*, n proceedings of *International Conference Dark Matter, Hadron Physics and Fusion Physics*, Messina Italy (2014) [*EPJ Web Conf.* **96** (2015) 01022] [INSPIRE].

[6] N.N. Achasov and A.A. Kozhevnikov, *Electromagnetic form factor of pion in the field theory inspired approach*, *Phys. Rev. D* **83** (2011) 113005 [*Erratum ibid.* **85** (2012) 019901] [arXiv:1104.4225] [INSPIRE].

[7] J.E. Augustin et al., *Study of Electron-Positron Annihilation into $\pi^+\pi^-$ at 775 MeV with the Orsay Storage Ring*, *Phys. Rev. Lett.* **20** (1968) 126 [INSPIRE].

[8] J.E. Augustin et al., *$\pi^+\pi^-$ production in e^+e^- collisions and $\rho - \omega$ interference*, in proceedings of *4th Rencontres de Moriond: Les Interactions Électromagnétiques*, Moriond France (1969) [*Lett. Nuovo Cim.* **2** (1969) 214].

[9] J.E. Augustin et al., *Study of electron-positron annihilation into $\pi^+\pi^-$ on the ρ-neutral resonance*, *Phys. Lett. B* **28** (1969) 508 [INSPIRE].

[10] V.L. Auslander, G.I. Budker, J.N. Pestov, V.A. Sidorov, A.N. Skrinsky and A.G. Khabakhpashev, *Investigation of the ϱ-meson resonance with electron-positron colliding beams*, *Phys. Lett. B* **25** (1967) 433 [INSPIRE].

[11] V.L. Auslander et al., *Investigation of the rho-meson resonance with electron-positron colliding beams*, *Yad. Fiz.* **9** (1969) 114 [*Sov. J. Nucl. Phys.* **9** (1969) 69]

[12] D. Benaksas et al., *$\pi^+\pi^-$ production by e^+e^- annihilation in the rho energy range with the Orsay storage ring*, *Phys. Lett. B* **39** (1972) 289 [INSPIRE].

[13] A. Quenzer et al., *Pion Form-Factor from 480 MeV to 1100 MeV*, *Phys. Lett. B* **76** (1978) 512 [INSPIRE].

[14] I.B. Vasserman et al., *Pion Form-Factor Measurement from $e^+e^- \to \pi^+\pi^-$ Near Threshold by electron-Positron Colliding Beams*, *Yad. Fiz.* **28** (1978) 968 [INSPIRE].

[15] A.D. Bukin et al., *Pion Form-Factor Measurement by $e^+e^- \to \pi^+\pi^-$ in the Energy Range 2 e from 0.78 GeV Up to 1.34 GeV*, *Phys. Lett. B* **73** (1978) 226 [INSPIRE].

[16] I.B. Vasserman et al., *Measurement of pion form-factor in $e^+e^- \to \pi^+\pi^-$ reaction near production threshold* (in Russian), *Yad. Fiz.* **30** (1979) 999 [*Sov. J. Nucl. Phys.* **30** (1979) 519] [INSPIRE].

[17] I.B. Vasserman et al., *Pion Form-factor Measurement in the Reaction $e^+e^- \to \pi^+\pi^-$ for Energies Within the Range From 0.4 GeV to 0.46 GeV*, *Yad. Fiz.* **33** (1981) 709 [*Sov. J. Nucl. Phys.* **33** (1981) 368]. [INSPIRE].

[18] L.M. Kurdadze et al., *Measurement of the pion form factor at* $640 \leq \sqrt{s} \leq 1400$ *MeV*, *JETP Lett.* **37** (1983) 733 [*Pisma Zh. Eksp. Teor. Fiz.* **37** (1983) 613] [INSPIRE].

[19] L.M. Kurdadze et al., *Study Of The Reaction* $e^+e^- \to \pi^+\pi^-$ *In The Energy Range From 640-mev - 1400-mev*, *Yad. Fiz.* **40** (1984) 451 [*Sov. J. Nucl. Phys.* **40** (1984) 286] [INSPIRE].

[20] S.R. Amendolia et al., *Measurement of the pion form-factor in the timelike region for* q^2 *values between* $0.1\,(GeV/c)^2$ *and* $0.18\,(GeV/c)^2$, *Phys. Lett. B* **138** (1984) 454 [INSPIRE].

[21] L.M. Barkov et al., *Electromagnetic Pion Form-Factor in the Timelike Region*, *Nucl. Phys. B* **256** (1985) 365 [INSPIRE].

[22] CMD-2 collaboration, *Measurement of* $e^+e^- \to \pi^+\pi^-$ *cross-section with CMD-2 around rho meson*, *Phys. Lett. B* **527** (2002) 161 [hep-ex/0112031] [INSPIRE].

[23] CMD-2 collaboration, *Update: A reanalysis of hadronic cross section measurements at CMD-2*, *Phys. Lett. B* **578** (2004) 285 [hep-ex/0308008] [INSPIRE].

[24] KLOE collaboration, *Measurement of* $\sigma(e^+e^- \to \pi^+\pi^-\gamma)$ *and extraction of* $\sigma(e^+e^- \to \pi^+\pi^-)$ *below 1 GeV with the KLOE detector*, *Phys. Lett. B* **606** (2005) 12 [hep-ex/0407048] [INSPIRE].

[25] M.N. Achasov et al., *Study of the process* $e^+e^- \to \pi^+\pi^-$ *in the energy region* $400 < \sqrt{s} < 1000$ *MeV*, *J. Exp. Theor. Phys.* **101** (2005) 1053 [hep-ex/0506076] [INSPIRE].

[26] M.N. Achasov et al., *Update of the* $e^+e^- \to \pi^+\pi^-$ *cross section measured by the spherical neutral detector in the energy region* $400 < \sqrt{s} < 1000$ *MeV*, *J. Exp. Theor. Phys.* **103** (2006) 380 [hep-ex/0605013] [INSPIRE].

[27] V.M. Aul'chenko et al., *Measurement of the* $e^+e^- \to \pi^+\pi^-$ *cross section with the CMD-2 detector in the 370–520-MeV c.m. energy range*, *JETP Lett.* **84** (2006) 413 [*Pisma Zh. Eksp. Teor. Fiz.* **84** (2006) 491] [hep-ex/0610016] [INSPIRE].

[28] CMD-2 collaboration, *High-statistics measurement of the pion form factor in the rho-meson energy range with the CMD-2 detector*, *Phys. Lett. B* **648** (2007) 28 [hep-ex/0610021] [INSPIRE].

[29] KLOE collaboration, *Measurement of* $\sigma(e^+e^- \to \pi^+\pi^-\gamma(\gamma)$ *and the dipion contribution to the muon anomaly with the KLOE detector*, *Phys. Lett. B* **670** (2009) 285 [arXiv:0809.3950] [INSPIRE].

[30] KLOE collaboration, *Measurement of* $\sigma(e^+e^- \to \pi^+\pi^-)$ *from threshold to 0.85 GeV*^{2} *using Initial State Radiation with the KLOE detector*, *Phys. Lett. B* **700** (2011) 102 [arXiv:1006.5313] [INSPIRE].

[31] KLOE-2 collaboration, *Measurement of the running of the fine structure constant below 1 GeV with the KLOE Detector*, *Phys. Lett. B* **767** (2017) 485 [arXiv:1609.06631] [INSPIRE].

[32] BaBar collaboration, *Precise measurement of the* $e^+e^- \to \pi^+\pi^-\gamma$ *cross section with the Initial State Radiation method at BABAR*, *Phys. Rev. Lett.* **103** (2009) 231801 [arXiv:0908.3589] [INSPIRE].

[33] BaBar collaboration, *Precise Measurement of the* $e^+e^- \to \pi^+\pi^-\gamma$ *Cross Section with the Initial-State Radiation Method at BABAR*, *Phys. Rev. D* **86** (2012) 032013 [arXiv:1205.2228] [INSPIRE].

[34] BESIII collaboration, *Measurement of the* $e^+e^- \to \pi^+\pi^-$ *cross section between 600 and 900 MeV using initial state radiation*, *Phys. Lett. B* **753** (2016) 629 [*Erratum ibid.* **812** (2021) 135982] [arXiv:1507.08188] [INSPIRE].

JHEP01(2021)113

[35] A.Yu. Barnyakov et al., *Testing aerogel Cherenkov counters with* $n = 1.05$ *using electrons and muons*, *Prib. Tekh. Eksp.* **1** (2015) 37 [*Instrum. Exp. Tech.* **58** (2015) 30].

[36] E.V. Abakumova et al., *A system of beam energy measurement based on the Compton backscattered laser photons for the VEPP-2000 electron–positron collider*, *Nucl. Instrum. Meth. A* **744** (2014) 35 [arXiv:1310.7764] [INSPIRE].

[37] E.V. Abakumova et al., *Backscattering of Laser Radiation on Ultrarelativistic Electrons in a Transverse Magnetic Field: Evidence of MeV-Scale Photon Interference*, *Phys. Rev. Lett.* **110** (2013) 140402 [arXiv:1211.0103] [INSPIRE].

[38] GEANT4 collaboration, *GEANT4 — a simulation toolkit*, *Nucl. Instrum. Meth. A* **506** (2003) 250 [INSPIRE].

[39] J. Allison et al., *Geant4 developments and applications*, *IEEE Trans. Nucl. Sci.* **53** (2006) 270 [INSPIRE].

[40] G.V. Fedotovich and A.I. Sibidanov, *Monte Carlo generator with radiative corrections for the* $e^+e^- \to e^+e^-, \mu^+\mu^-$ *and* $\pi^+\pi^-$ *processes at low energies*, *Nuc. Phys. B Proc. Suppl.* **131** (2004) 9

[41] A.B. Arbuzov, G.V. Fedotovich, E.A. Kuraev, N.P. Merenkov, V.D. Rushai and L. Trentadue, *Large angle QED processes at* e^+e^- *colliders at energies below 3 GeV*, *JHEP* **10** (1997) 001 [hep-ph/9702262] [INSPIRE].

[42] A.B. Arbuzov, V.A. Astakhov, A.V. Fedorov, G.V. Fedotovich, E.A. Kuraev and N.P. Merenkov, *Radiative corrections for pion and kaon production at* e^+e^- *colliders of energies below 2 GeV*, *JHEP* **10** (1997) 006 [hep-ph/9703456] [INSPIRE].

[43] M.N. Achasov, K.I. Beloborodov and A.S. Kupich, *Separation of* $e^+e^- \to e^+e^-$ *and* $e^+e^- \to \pi^+\pi^-$ *events using SND detector calorimeter*, 2017 *JINST* **12** T01002 [arXiv:1611.07729] [INSPIRE].

[44] CMD-3 collaboration, *Search for the process* $e^+e^- \to \eta'958$ *with the CMD-3 detector*, *Phys. Lett. B* **740** (2015) 273 [arXiv:1409.1664] [INSPIRE].

[45] M.N. Achasov et al., *Study of the process* $e^+e^- \to \pi^+\pi^-\pi^0$ *in the energy region* $\sqrt{s}$ *below 0.98 GeV*, *Phys. Rev. D* **68** (2003) 052006 [hep-ex/0305049] [INSPIRE].

[46] PARTICLE DATA GROUP collaboration, *Review of Particle Physics*, *Phys. Rev. D* **98** (2018) 030001 [INSPIRE].

[47] K. Hagiwara, R. Liao, A.D. Martin, D. Nomura and T. Teubner, $(g-2)_\mu$ *and* $\alpha(M_Z^2)$ *re-evaluated using new precise data*, *J. Phys. G* **38** (2011) 085003 [arXiv:1105.3149] [INSPIRE].

[48] F. Ignatov, https://cmd.inp.nsk.su/~ignatov/vpl/.

[49] J. Schwinger, *Particles, Sources and Fields. Vol. II*, *Advanced Book Program*, Addison-Wesley Publishing Company, Reading U.S.A. (1973).

[50] KLOE-2 collaboration, *Combination of KLOE* $\sigma(e^+e^- \to \pi^+\pi^-\gamma(\gamma))$ *measurements and determination of* $a_\mu^{\pi^+\pi^-}$ *in the energy range* $0.10 < s < 0.95\,GeV^2$, *JHEP* **03** (2018) 173 [arXiv:1711.03085] [INSPIRE].

[51] KLOE collaboration, *Study of the decay* $\phi \to \pi^+\pi^-\pi^0$ *with the KLOE detector*, *Phys. Lett. B* **561** (2003) 55 [*Erratum ibid.* **609** (2005) 449] [hep-ex/0303016] [INSPIRE].

JHEP01(2021)113